Bollettino di Geofisica Teorica ed Applicata Vol. 60, n. 4, pp. 621-628; December 2019
DOI 10.4430/bgta0278

Joint constrained inversion of TEM data to investigate deeply-buried ore deposit

J. Xue[1], Y. Lu[2], G. Xue[3,4,5], W. Chen[3,4,5], K. Lei[3,4,5], M.Y. Khan[6] and H. Wang[7]

[1] *College of Geoscience and Surveying Engineering, China University of Mining and Technology, Beijing, China*

[2] *PowerScan Company Limited Beijing, China*

[3] *Key Laboratory of Mineral Resources, Institute of Geology and Geophysics, Chinese Academy of Sciences, Beijing, China*

[4] *Institution of Earth Science, Chinese Academy of Sciences, Beijing, China*

[5] *University of the Chinese Academy of Sciences, Beijing, China*

[6] *National Centre of Excellence in Geology, University of Peshawar, Pakistan*

[7] *Shandong Bureau of Coal Geology, Jinan, China*

(Received: 24 December 2018; accepted: 18 April 2019)

ABSTRACT Theoretically, the grounded-wire transient electromagnetic method can obtain five different components in field measurements for deep ore deposit exploration. The electrical component usually offers high precision and detection depth as compared to the magnetic component due to stronger anti-noise ability, while the magnetic component has the merit of stability in the inversion process but is insensitive to the resistance body. Considering that the Gram constraint is a kind of generalised constraint, applied for components of non-linear relation, this paper proposes a joint constrained inversion method to combine the electrical and magnetic component data, which are inverted by a truncated singular value decomposition method. Finally, the conjugate gradient inversion method is applied to synthetic data and iron ore field data to demonstrate the improved result based on both the electrical and magnetic component.

Key words: SOTEM, response analysis, joint constrained inversion, multi-component, high precision.

1. Introduction

The ground-based short-offset transient electromagnetic method (SOTEM) has gained popularity as a newly developing transient electromagnetic method (TEM) over the last few years in China. In this method, the grounded wire is used as a source to detect a buried target at a depth equal to or less than the separation between source and receiver (Xue *et al*., 2013, 2014). SOTEM has been widely used in hydrogeological and mineral exploration (Evan *et al*., 2012; Chen *et al*., 2016a, 2016b, 2017b; Zhou *et al*., 2016) due to its large detection depth (500-2000 m), and as a result, it has high detection sensitivity to both low and highly resistant targets (Li *et al*., 2015) compared to loop source TEM. SOTEM also offers high efficiency, especially in mountainous areas.

The accurate data processing technology is the key step to ensure the deep detection capability of grounded-wire electromagnetic exploration (Bouchedda *et al*., 2010). Literature

shows that different inversion schemes have been applied to electric source TEM measurements. Strack (1992) and Khan *et al*. (2018) discussed the Occam inversion of LOTEM data. Chen *et al*. (2017a) proposed an Occam scheme to invert the vertical magnetic field component of SOTEM, and applied it to synthetic and field data.

Loess deposits are widely distributed in China. These deposits are very conductive in nature and may conceal coal seams with hundreds of metres thick overburden. Therefore, the rough topography and complex geological setting in northern China demand an advance in geophysical techniques and an improvement in processing routines. Five components of the EM field are observed in a SOTEM survey, including two horizontal components (electric and magnetic field) and one vertical magnetic field component. It is common practice to invert SOTEM data using only magnetic component, which limits the detection depth. The multi-component inversion method combines the detection advantages of each component, making it an inevitable choice for improved understanding based on joint inversion. Several studies have demonstrated the successful application of joint inversion (Davood *et al*., 2015).

Sasaki (1989) introduced the constrained least squares method by carrying out a two-dimensional joint inversion of the magnetotelluric and dipole-dipole method, and produced reasonable results. Meju (1995) performed the joint inversion of magnetotelluric data and transient electromagnetic data by setting different weighting coefficients. Mackie *et al*. (2007) carried out a 3D joint inversion of controlled source data and magnetotelluric data. Pieta and Bala (2008) performed the joint inversion of DC electromagnetic depth data and electromagnetic data using the Monte Carlo global optimisation algorithm.

Using more than one EM field component increases the reliability of the inversion result (Strack, 1992) due to their varying sensitivity to different subsurface targets. In order to make full use of the information contained in different electromagnetic field components, a multi-component joint constrained inversion is proposed and has proved an effective way to invert the multi-component SOTEM data. At present, 2D and 3D modelling techniques are in the stage of development for the SOTEM method. Therefore, we have sought to achieve improved and reliable results based on the one-dimensional forward operator in the joint inversion of SOTEM soundings (Cai *et al*., 2014).

2. Inversion methods

The relationship between observed data and geological model parameters is:

$$\mathbf{d} = \mathbf{A}(\mathbf{m}) \tag{1}$$

where **d** denotes field survey data, **m** denotes geological parameters, **A** denotes operator matrix.

The geological parameters can be inverted by regularisation, in which objective function **F** is defined as follows:

$$\min \mathbf{F} = \mathbf{F_d}(\mathbf{m}) + \alpha \mathbf{F_m}(\mathbf{m}) \tag{2}$$

where, $\mathbf{F_d}(\mathbf{m}) = \sum_{i=1}^{n} (\mathbf{d}_i - \mathbf{A}_i(\mathbf{m}))^2$, $\mathbf{F_m}(\mathbf{m}) = \sum_{i=1}^{n} \left\| \mathbf{m}^i \right\|^2$, α denotes regularisation parameter.

2.1. Truncated singular value decomposition inversion method

The truncated singular value decomposition (TSVD) technique is a widely used regularisation approach of direct solution method, which is based on matrix decomposition, and can solve small and medium-size linear discrete ill-posed equations. When the discrete Picard condition is satisfied, a smooth result, which is similar to the Tikhonov regularisation, can be obtained (Christian, 1990).

Applying the singular value decomposition (SVD) method to the operator **A** in Eq. 1, we can write it as follows (Lin *et al*., 2017):

$$\mathbf{A} = \mathbf{U}_r \mathbf{\Sigma}_r \mathbf{S}_r^T \tag{3}$$

where $\mathbf{U}_r$ is p×r order matrix, $\mathbf{S}_r$ is q×r order matrix, $\mathbf{\Sigma}_r$ is r×r order diagonal matrix as well as the singular value matrix.

Based on the SVD technique, TSVD can solve the ill-posed equations. It keeps large singular values unchanged and truncates small singular values to eliminate the influence of these on the solution.

Assuming k is the truncated position, λ_k is the corresponding truncated parameters, so the truncated singular matrix $\mathbf{\Sigma}_r^k$ can be expressed as:

$$\sum\nolimits_r^k = \begin{bmatrix} \lambda_1 & 0 & 0 & 0 & \cdots & 0 \\ 0 & \ddots & 0 & 0 & \cdots & 0 \\ 0 & 0 & \lambda_r & 0 & \cdots & 0 \\ 0 & 0 & 0 & 0 & \cdots & 0 \end{bmatrix} \tag{4}$$

and the solution of Eq. 1 by TSVD is:

$$\mathbf{m} = \mathbf{S}_r \mathbf{\Sigma}_r^k \mathbf{U}_r^T \mathbf{d} \tag{5}$$

The key to the TSVD method is how to determine the truncated position and parameters. In this paper, the generalised cross-validation (GCV) is used to determine the truncation parameters. The GCV function is (Lin *et al*., 2017):

$$\lambda_k = \arg\min \frac{p\left\|(\mathbf{I} - \mathbf{H}_\lambda)\mathbf{d}\right\|^2}{[tr(\mathbf{I} - \mathbf{H}_\lambda)]^2} \tag{6}$$

where p is observation number, $\mathbf{I}$ is a unit matrix, $\mathbf{H}_\lambda = \mathbf{A}\mathbf{S}_r\mathbf{\Sigma}_r^k\mathbf{U}_r^T$ can be seen as the influence matrix, which satisfies $\mathbf{Am} = \mathbf{H}_\lambda\mathbf{d}$. The truncated parameters can be obtained by minimalising the GCV function.

2.2. Constrained inversion

In this paper, the Gram matrix can be expressed as:

$$S_G(\mathbf{m}^1, \mathbf{m}^2) = \begin{vmatrix} (\mathbf{m}^1, \mathbf{m}^1) & (\mathbf{m}^1, \mathbf{m}^2) \\ (\mathbf{m}^2, \mathbf{m}^1) & (\mathbf{m}^2, \mathbf{m}^2) \end{vmatrix}. \tag{7}$$

Using TSVD method, $\mathbf{m}^1$ and $\mathbf{m}^2$ inversed by $\mathbf{d}^1$ and $\mathbf{d}^2$ respectively, after that, the constraint function of joint inversion can be established by Gram matrix.

The objective function of joint inversion can be expressed as follows (Yu *et al*., 2009; Li *et al*., 2015):

$$\mathbf{F} = \sum_{i=1,2} \left\| \mathbf{W}_d^i (\mathbf{A}^i(\mathbf{m}^i) - \mathbf{d}^i) \right\|^2 + \sum_{i=1,2} \lambda^i \left\| \mathbf{W}_m^i (\mathbf{m}^i) \right\|^2 + \beta \mathbf{S}_G \tag{8}$$

where $\mathbf{W}_d^i$ and $\mathbf{W}_m^i$ are weight matrix, which can normalise the model data or fitting error:

$$\mathbf{W}_m^i = \frac{1}{\max |\mathbf{m}^i|}, \ \mathbf{W}_d^i = diag\left(\frac{1}{\left\| A^i(\mathbf{m}^i) - \mathbf{d}^i \right\|}\right) \tag{9}$$

In order to obtain the minimum value of Eq. 8, the first order variation of the objective function is:

$$\delta \mathbf{F} = 2 \sum_{i=1,2} (\delta \mathbf{m}^i) \mathbf{l}^i, \qquad i = 1, 2. \tag{10}$$

where:

$$\mathbf{I}^i = (\mathbf{A}_j^i)\ (\mathbf{W}_d^i)^2\ \mathbf{r}^i + \alpha^i\ (\mathbf{W}_m^i)\ (\mathbf{m}^i) + \lambda \mathbf{G}^i \mathbf{m}^i \tag{11}$$

$$\begin{aligned} \mathbf{G}^1 &= (\mathbf{T}^1)[(\mathbf{m}^2)(\mathbf{m}^2)\mathbf{I} - (\mathbf{m}^2)(\mathbf{m}^2)]\mathbf{T}^1 \\ \mathbf{G}^2 &= (\mathbf{T}^2)[(\mathbf{m}^1)(\mathbf{m}^1)\mathbf{I} - (\mathbf{m}^1)(\mathbf{m}^1)]\mathbf{T}^1 \end{aligned} \tag{12}$$

$\mathbf{A}_j^i$ is the Jacobi matrix of $\mathbf{A}^i$, $\mathbf{T}^1$ and $\mathbf{T}^2$ are custom operators, $\mathbf{r}^i$ is a fitting error:

$$\mathbf{r}^i = \mathbf{A}^i(\mathbf{m}^1) - \mathbf{d}^i. \tag{13}$$

Eq. 10 is a linear function, so the conjugate gradient method can be used to obtain the optimal value.

3. Synthetic data inversion

In order to verify the effectiveness of the joint constrained inversion, a five-layer model (HKH model) is constructed for the vertical magnetic and horizontal electric component (Figs. 1a and 1b) as well as the multi-component (Hz and Ex) data (Fig. 1c). For both cases, the modelling parameters of SOTEM include the length of the transmitter of 1000 m, emission current of 10 A, offset and sampling time of 1000 m and 10 ms.

Fig. 1 shows the comparison of single-component and multi-component joint inversion of the HKH model. The inversion results of the magnetic field component (dHz/dt) and the electric field components are shown in Figs. 1a and 1b, respectively. Fig. 1c shows the joint inversion result of electric and magnetic field component after 1, 3, 6, and 8 iterations. As can be seen from Fig. 1c, joint inversion provides the result that almost reflects the actual model after performing the third iteration. Thus, joint inversion gives a better result than the one using a

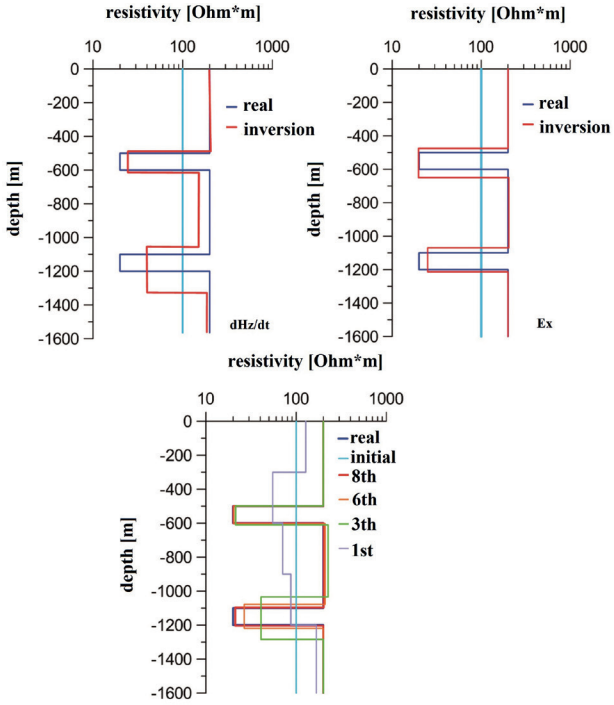

Fig. 1 - Joint inversion and single inversion of dHz/dt and Ex for HKH model: a) inversion result of magnetic field component dHz/dt; b) inversion result of electric field component Ex; c) joint inversion result.

single EM field component (Figs. 1b and 1c).

Fig. 2 shows a single component and multicomponent constrained inversion profiles. Both the TSVD inversion results of an electric (Fig. 2a) and magnetic component (Fig. 2b) demonstrate a distorted picture of the target layers in terms of thickness and depth parameters. However, the results of the multi-component joint constrained inversion (Fig. 2c) clearly resolved the subsurface structure where geoelectrical layers reflect the actual model.

4. Field data inversion

The survey area is located in Dezhou City, Shandong province, where large quantities of iron ore have been discovered. The ZK1 borehole reveals 4 layers of magmatic rock, the total thickness of the ore body ranging from 5.30 to 123.46 m.

To acquire detailed subsurface information on the depth and lateral extension of the buried iron ore body, SOTEM electromagnetic soundings were carried out. Due to the considerable coverage of low-resistance layers within the urban area, it became difficult to collect deeper information based on a single field component. Therefore, both the vertical magnetic field and horizontal electric field components are collected as shown in Fig. 3.

The survey was set up with the following parameters: transmitter length 1000 m; transmitter-receiver distance 1100 m; emission current 14 A; base frequency 1 Hz; profile length 1800 m; point interval 40 m; effective receiving area 10,000 m^2. The vertical induction EMF dBz/dt and the horizontal electric field Ex component were collected along two SOTEM profiles (L1 and L2).

Fig. 4 shows the decay curves of the measured magnetic and electric components. The data of the dBz/dt component are greatly influenced by electromagnetic noise (Fig. 4a). However,

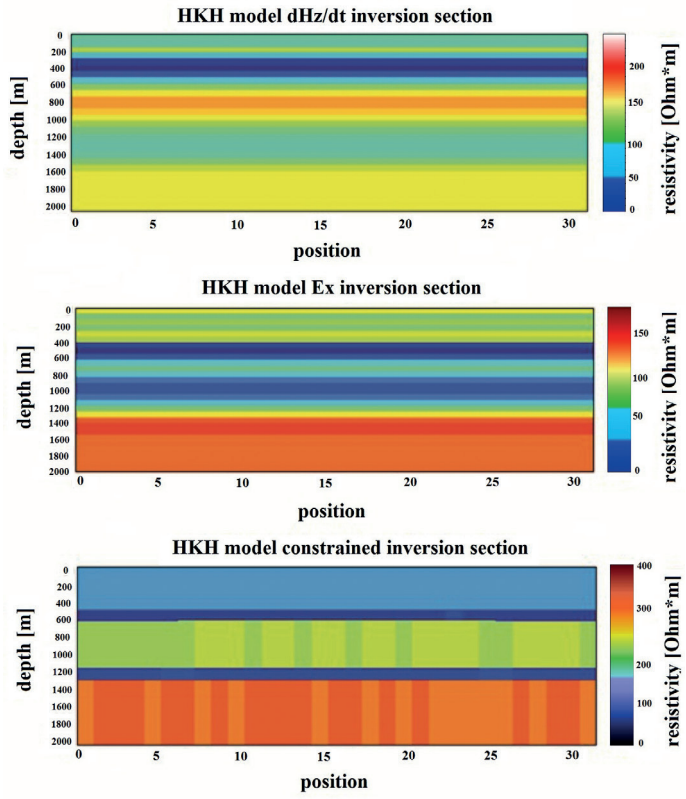

Fig. 2 - Joint inversion and single inversion of dHz/dt and Ex for KHK model: a) TVSD inversion section of magnetic field component dHz/dt; b) TVSD inversion section of electric field component Ex; c) joint inversion section of magnetic and electric field component dHz/dt, Ex.

the decay curves of the electric field component Ex are smoother than that of dBz/dt component, which means that Ex has a strong anti-noise ability (Fig. 4b).

Fig. 5b indicates noise contaminating the electric field component Ex at 700, 1100 and 1700 m due to the strong impact of external sources in the surroundings and or topography and induced polarization. By comparing the multi-channel shown in Figs. 5a and 5b, it can be seen that the electric field signals of some measuring points of L1-line are distorted, which may be affected by topography and induced polarization.

The constrained inversion results are shown in Fig. 6. The inversed resistivity cross-section reflects four distinct geological layers in the central part of the profile. The anomalous body can be observed at 1300-1800 m within a depth range of 1000 to 1600 m. We interpret this high

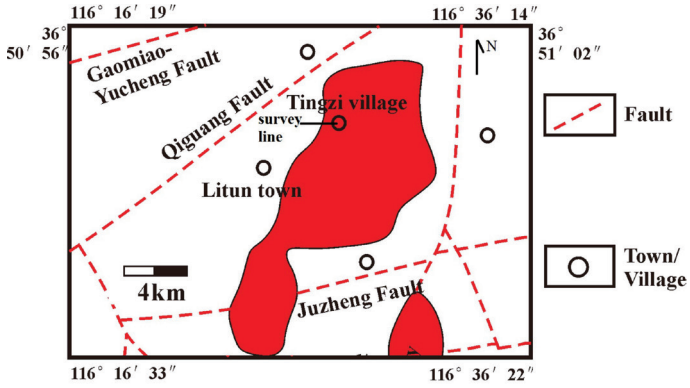

Fig. 3 - The device line of SOTEM in the survey area.

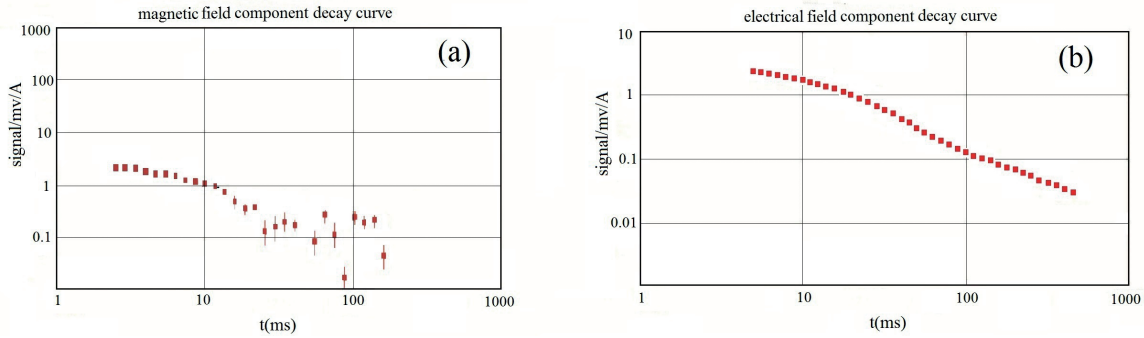

Fig. 4 - Decay curves of the SOTEM Ex and dBz/dt component: a) decay curve of measured data dBz/dt; b) decay curve of measured data Ex.

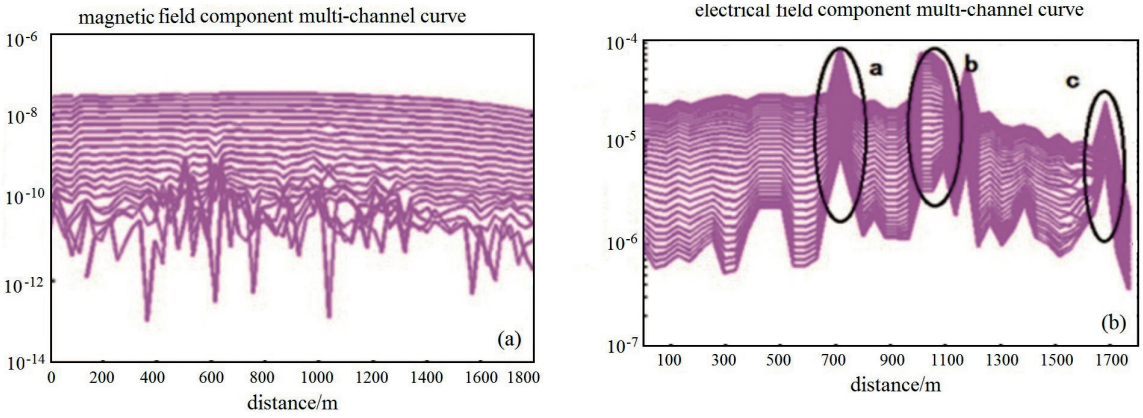

Fig. 5 - Ex and dHz/dt component multi-channel curves of line L1: a) dBz/dt component multi-channel curves b) Ex component multi-channel curves.

resistivity zone as a potential prospect of iron-ores deposited in Ordovician and carboniferous limestone due to the magmatic intrusion, which is subsequently confirmed through drilling information available in the region.

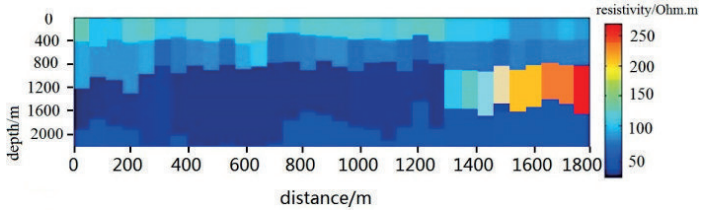

Fig. 6 - dHz/dt and Ex component constrained inversion profile of line L1.

5. Conclusion

In this paper, we have shown that the joint constrained inversion approach is feasible for inverting SOTEM data to study iron-ore deposits. In grounded-wire SOTEM, it is beneficial to utilise the advantages of different components by joint inversion, which can increase the

accuracy of inversion and reduce the contaminating noise due to various internal and external sources. Therefore, we use the Gram matrix to build a constrained term to combine the inverted data from vertical magnetic field component and the horizontal electric field component. Based on the field data results, we infer that joint constrained inversion can resolve buried ore-deposits better than the inversion of TEM data relying solely on a single component of the EM field.

Acknowledgements. This research study is supported by the National Key Research and Development Program of China (2017YFC0601204) and the Natural Science Foundation of China (NSFC) (41830101).

REFERENCES

Bouchedda A., Chouteau M., Keating P. and Smith R.; 2010: *Sferics noise reduction in time-domain electromagnetic systems: application to megatemii signal enhancement*. Explor. Geophys., **41**, 225-239.

Cai J., Qi Y.F. and Yin C.C.; 2014: *Weighted Laterally-constrained inversion of frequency-domain airborne EM data*. Chin. J. Geophys., **57**, 953-960.

Chen W.Y., Xue G.Q., Cui J.W. and Zhong H.S.; 2016a: *Study on the response and optimal observation area for SOTEM*. Chin. J. Geophys., **59**, 739-748.

Chen W.Y., Xue G.Q., Khan M.Y. and Li H.; 2016b: *Using SOTEM method to detect bif bodies buried under very thick and conductive quaternary sediments, huoqiu deposit*. Pure Appl. Geophys., **174**, 1013-1023.

Chen W.Y., Li H., Xue G.Q., Chen K. and Zhong H.S.; 2017a: *1D OCCAM inversion of SOTEM data and its application to 3D models*. Chin. J. Geophys., **60**, 3667-3676.

Chen W.Y., Xue G.Q. and Afolagboye L.Ol.; 2017b: *A comparison of loop TEM and SOTEM methods for mapping water-enriched zones - A case history in Shaanxi, China*. Geophys., **82,** B201-B208.

Christian H.P.; 1990: *Truncated singular value decomposition solutions to discrete Ill-posed problems with Ill-determined numerical rank*. Siam J. Sci. Stat. Comput., **11**, 503-518.

Davood M., Martin E. and Katrin S.; 2015: *1D joint multi-offset inversion of time-domain marine controlled source electromagnetic data*. Geophys. Prospect., **63**, 1334-1354.

Evan S.U., David A., Jerry M.H. and Chen J.P.; 2012: *Numerical modeling analysis of short-offset electric-field measurements with a vertical electric dipole source in complex offshore environments*. Geophys., **77**, E329-E341.

Khan M.Y., Xue G., Chen W. and Zhong H.; 2018: *Analysis of long-offset transient electromagnetic (LOTEM) data in time, frequency, and pseudo-seismic domain*. J. Environ. Eng. Geophys., **23**, 15-32.

Li X., Liu W.T., Zhi Q.Q. and Zhao W.; 2015: *Three-dimensional joint interpretation of nuclear magnetic resonance and transient electromagnetic data*. Chin. J. Geophys., **58**, 2730-2744.

Lin D.F., Zhu J.J. and Song Y.C.; 2017: *Truncation method for TSVD with account of truncation bias*. Acta Geod. Cartogr. Sin., **46**, 679-688.

Mackie R., Watts M.D. and Rodi W.; 2007: *Joint 3d inversion of marine CSEM and MT data*. In: Expanded Abstracts 77th SEG International Exposition and Annual Meeting, San Antonio, TX, USA, 26, pp. 574-578.

Meju J.M.; 1995: *Simple effective resistivity depth transformations for infield or real-time data processing*. Comput. Geosci., **21**, 985-992.

Pieta A. and Bala J.; 2008: *Validation of joint inversion of direct current and electromagnetic measurements*. Acta Geophys., **58**, 114-125.

Sasaki Y.; 1989: *Two-dimensional joint inversion of magnetotelluric and dipole-dipole resistivity data*. Geophys., **54**, 254-262.

Strack K.M.; 1992: *Exploration with deep transient electromagnetics*. Elsevier, 373 pp.

Xue G.Q., Chen W.Y., Zhou N.N. and Li H.; 2013: *Short-offset TEM technique with a grounded wire source for deep sounding*. Chin. J. Geophys., **56**, 255-261.

Xue G.Q., Gelius L.J., Sakyi P.A., Zhou N.N., Chen W.Y., Su B.C., Li H., Zhong H.S. and Su Y.P.; 2014: *Discovery of a hidden BIF deposit in Anhui province, China by integrated geological and geophysical investigations*. Ore Geol. Rev., **63**, 470-477.

Yu P., Dai M.G., Wang J.L. and Wu J.S.; 2009: *Joint inversion of magnetotelluric and seismic data based on random resistivity and velocity distributions*. Chin. J. Geophys., **52**, 1089-1097.

Zhou N.N., Xue G.Q., Chen W.Y. and Cheng J.; 2016: *Large-depth hydrogeological detection in the north China-type coalfield through short-offset grounded-wire TEM*. Environ. Earth Sci., **74**, 2393-2404.

Corresponding author: Guoqiang Xue
Institute of Geology and Geophysics, Chinese Academy of Science
19 North Tucheng West Road, Beijing 100029, China
Phone: +86 13146176332; e-mail: ppxueguoqiang@163.com